



ARTICLE

Open Access

# Cantilever beam-based piezoelectric micromachined ultrasonic transducer with post processing soft interconnecting strategy for in-air rangefinding

Yan Wang<sup>1,2</sup> , Peng Chen<sup>1,2</sup>, Junning Zhang<sup>1</sup>, Zihan Li<sup>1</sup> and Hongbin Yu<sup>1,2,3</sup> ✉

## Abstract

Despite of good performance immunity to stress and high transmitting/receiving sensitivity advantages, the fabrication imperfection induced asynchronous vibration and the resultant prolonged ring-down tail severely limit the potential of the cantilever beam-based piezoelectric micromachined ultrasonic transducer (PMUT) in pulse-echo applications as transceiver. To address this issue, a novel post processing soft interconnecting strategy is presented. In this case, specific reservoir structure is intentionally integrated into the cantilever-beam based PMUT design, under the assistance of which the liquid PDMS can be accurately applied and spontaneously driven to seal the air gaps between the already released cantilever beams via the capillary effect. After curing, the PDMS will be transformed from liquid to solid and serve as soft interconnecting spring between adjacent cantilever beams so as to force them to vibrate in synchronous mode. At the same time, this treatment does not change the existing fabrication process and has little effect on the original PMUT performance. From both of the mechanical and acoustic response measurement results, effective suppression for the asynchronous vibration and significant reduction of the ring-down tail have been successfully demonstrated for the treated PMUT device. In the subsequent pulse-echo rangefinding experiment, a distance detection range covering from 270.8 mm to 3.8 m with a divergence angle close to 170° has been achieved when it is driven at resonant frequency of 69.2 kHz with 40  $V_{pp}$ , 40-cycles sinusoidal signal. Given the simple yet effective treatment, the proposed strategy shows great prospective in developing high performance PMUT for in-air rangefinding applications.

## Introduction

To meet the rapidly evolving demands of industrial development and emerging application scenarios, as the key sensing modules used in intelligent electronic devices, collaborative robots and drones to obtain target position information, the rangefinders have been expecting to provide higher performance standards. Among the existing rangefinder technologies, the optical methods face difficulty in detecting transparent/dark-colored objects

and are highly susceptible to ambient light interference<sup>1</sup>, whilst the traditional piezoelectric ceramic-based ultrasonic ones are limited by large size, high power consumption and poor acoustic coupling<sup>2</sup>. The advancement of micro-electromechanical systems (MEMS) technology has led to the development of capacitive micromachined ultrasonic transducer (CMUT) and PMUT. However, CMUT faces challenges such as high bias voltage requirement, nonlinear response mechanism and narrow electrode gap, which led to complicated operation control and limited displacement for rangefinder applications<sup>3</sup>. In contrast, PMUT offers advantages including simple structure, linear control and large displacement, making it a promising candidate in air-coupled ultrasonic sensing applications<sup>4–7</sup>.

Correspondence: Hongbin Yu ([yuhb@hust.edu.cn](mailto:yuhb@hust.edu.cn))

<sup>1</sup>School of Optical and Electronic Information, Huazhong University of Science and Technology, Wuhan 430074, China

<sup>2</sup>Optics Valley Laboratory, Hubei 430074, China

Full list of author information is available at the end of the article

© The Author(s) 2025



**Open Access** This article is licensed under a Creative Commons Attribution-NonCommercial-NoDerivatives 4.0 International License, which permits any non-commercial use, sharing, distribution and reproduction in any medium or format, as long as you give appropriate credit to the original author(s) and the source, provide a link to the Creative Commons licence, and indicate if you modified the licensed material. You do not have permission under this licence to share adapted material derived from this article or parts of it. The images or other third party material in this article are included in the article's Creative Commons licence, unless indicated otherwise in a credit line to the material. If material is not included in the article's Creative Commons licence and your intended use is not permitted by statutory regulation or exceeds the permitted use, you will need to obtain permission directly from the copyright holder. To view a copy of this licence, visit <http://creativecommons.org/licenses/by-nc-nd/4.0/>.

The PMUT-based rangefinders can capture the distance information by measuring the time of flight of the ultrasonic signal. Compared to the rangefinder counterparts that use two individual PMUT units to transmit and receive ultrasonic signal separately<sup>7–9</sup>, the self-transceiving configuration can achieve these functions with the same unit<sup>2</sup>. Obviously, the less number of the PMUTs help to reduce the system volume and cost, and enhance application flexibility. Most importantly, since both of the signal transmission and reception are conducted by the same PMUT, there is no need to consider the frequency consistency between the transmitting and receiving units, thus largely simplifying the fabrication process control<sup>10</sup>. According to the electromechanical transduction structure design, the PMUT can be roughly categorized into three types, namely fully-closed PMUT<sup>2,11,12</sup>, quasi-closed PMUT<sup>13–16</sup> and cantilever beam-based PMUT<sup>17–19</sup>. Traditional fully-closed PMUT consists of a fully-closed diaphragm anchored to the substrate on all sides, offering advantages such as simple structure, relatively simple fabrication processes, and excellent acoustic sealing. However, the fully-closed PMUT is highly sensitive to stress, which can lead to nonlinear effects during deformation and a reduction in device sensitivity<sup>20</sup>. Moreover, the process related residual stress in the as-deposited material will largely change the mechanical performance of the fully-closed structure, causing uniformity issue<sup>17</sup>. Quasi-closed PMUT incorporates open structures such as through-holes or slits, which can partially relieve the diaphragm internal stress and provide greater design flexibility, enabling performance tuning capability for device such as bandwidth. However, its performance is still considerably influenced by the residual stress, making process control critical<sup>16</sup>. In contrast, the cantilever structure can effectively release stress through its deformation, making its performance insensitive to fabrication-induced residual stress and thereby easily achieving high fabrication consistency. Moreover, due to the mechanical characteristic of the structure, the cantilever beam-based PMUT exhibits larger linear operation range and higher operation sensitivity<sup>18,19</sup>. As a result, it is highly suitable for high SNR and long distance detection scenario.

Considering the fact that the cantilever performance is dependent on its structure, any dimension deviation caused by fabrication will lead to varied resonant frequencies across multiple cantilever beams in a PMUT. Since the response will undergo significant phase changes when the cantilever is driven to vibrate at its resonant frequency, asynchronous vibration between inconsistent cantilevers will happen under the same driving signal due to their resonant frequency difference<sup>18</sup>. On the one hand, the sound radiation energy will continuously couple between cantilevers after the driving signal is switched off

under the effect of the asynchronous vibration, resulting in prolonged ring-down time for settling down. As for the self-transceiving configuration, it's well known that the echo signal can only be distinguished when the ring-down amplitude is reduced to a certain level, which corresponds to an important performance indicator for the rangefinder, namely the detection blind area. Obviously, the increased ring-down time will expand the blind area. On the other hand, the emitted sound pressures from the asynchronously vibrating cantilevers cannot be superposed constructively or even might be canceled out by each other in the worst case, thus decreasing the emitted sound pressure level as well as the maximum detection range.

To address the asynchronous vibration issues, Gong et al. introduced mechanical coupling beams between cantilevers as hard connection spring for asynchronous vibration suppression<sup>18</sup>. In this case, in order to obtain effective suppression, the coupling beams should be arranged close to the cantilever tip region. However, this will increase both of the structure stiffness and the performance sensitivity to stress, resulting in reduced operation sensitivity and linear working range as well. Furthermore, the existence of the coupling beams can not only influence the release of residual stress in the cantilevers during fabrication, but also alter the stress distribution within the cantilever and lead to incomplete electrode coverage of the piezoelectric layer, deteriorating PMUT performance further.

In our previous work, a capillary effect-based post processing autonomous sealing method was firstly developed and successfully applied to the piezoelectric MEMS speaker to suppress the asynchronous vibration between cantilevers and improve its broadband sound pressure output performance<sup>21</sup>. Although the working frequency and the detailed impact on the device performance are a bit different, this strategy should be still applicable to PMUT due to the similar operation mechanism. For proof of concept demonstration, a cantilever-based PMUT for in-air rangefinder is developed, in which four liquid reservoir structures connected to the air gaps are intentionally designed at the corner of device to facilitate spontaneous and reliable filling of the air gaps by the liquid PDMS through the capillary effect and provide accurately confined liquid spread. After curing, the filled PDMS will be transformed from liquid to solid and act as solid soft interconnecting springs between cantilever beams, forcing them to vibrate in synchronous mode. The device performance change before and after treatment are investigated by simulation and experiment. From the results, it can be seen that after sealing, the originally existed multiple resonance peaks in the as-fabricated PMUT will be merged into one and the ring-down time can be significantly shortened, representing

effective suppression of the asynchronous vibration. When driven by a 40-cycles sinusoidal signal with 40  $V_{pp}$  at the device's resonant frequency, the blind area of the developed self-transceiving PMUT rangefinder can be remarkably decreased from larger than 1 m to 270.8 mm. In addition, it can also be found that this method demonstrates less impact on the original high emission sensitivity of the PMUT and achieve a maximum detection range up to 3.8 m despite of small device footprint.

## Materials and methods

### Structure design

Figure 1a shows the schematic of the proposed cantilever beam-based PMUT. It consists of four identical triangular piezoelectric cantilever beams, which are arranged into a square shape and electrically connected together for simultaneous actuation. The composite film stack of the piezoelectric cantilever, from top to bottom, is 200 nm  $\text{Si}_3\text{N}_4$ , 200 nm Mo, 1  $\mu\text{m}$  AlN, 200 nm Mo and 3  $\mu\text{m}$  Si. The side length of the cantilever beams and the width of the air gap between them are designed to be 720  $\mu\text{m}$  and 2  $\mu\text{m}$ , respectively. The air gap between the cantilever beams serves as suspended channel<sup>22</sup>, creating a capillary path. Once the PMUT is fabricated, the liquid PDMS will be injected into the reservoir with a diameter of 120  $\mu\text{m}$  using a dispensing machine, and it will spontaneously fill into the air gap region, driven by the capillary force. In this step, the PDMS is selected as the sealing material due to its low surface energy in liquid status and low Young's modulus (750 kPa) as well as excellent elasticity in solid status. After complete curing, the solid PDMS will act as a soft spring that connects the adjacent cantilever beams and forces them to vibrate synchronously. Moreover, the PDMS will also seal the air gaps, thus preventing the

PMUT performance from being changed by any process-induced dimension deviation. At the same time, as a post-release process, this sealing operation will not interfere with the existing PMUT fabrication process or affect the residual stress release of the cantilever beams.

The PMUT can be modeled as a one-dimensional spring-mass-damping system. Upon sinusoidal excitation at the operating frequency of  $\omega$ , the motion equation of the PMUT can be expressed as:

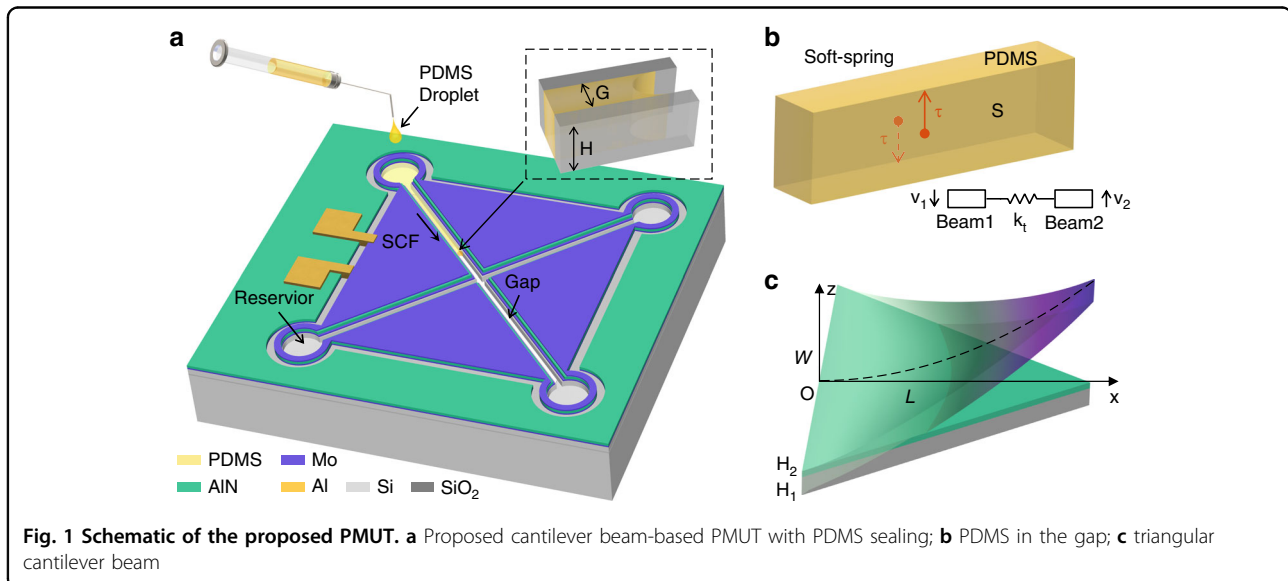
$$\begin{cases} \ddot{z} + \frac{R}{M}\dot{z} + \frac{K}{M}z = \frac{F_0}{M}\sin(\omega t) \\ z(0) = z_0, \dot{z}(0) = \dot{z}_0 \end{cases} \quad (1)$$

where  $M$ ,  $K$ , and  $R$  are the equivalent mass, the equivalent spring constant and the damping of the PMUT, respectively.  $F_0$  is force amplitude.  $z_0$  and  $\dot{z}_0$  represent the initial displacement and initial velocity of the PMUT, respectively.

Its solution is given by<sup>23</sup>:

$$\begin{cases} z(t) = z_1(t) + z_2(t) + z_3(t) \\ z_1(t) = e^{-\xi\omega_0 t} \left( z_0 \cos \omega_d t + \frac{\dot{z}_0 + \xi\omega_0 z_0}{\omega_d} \sin \omega_d t \right) \\ z_2(t) = B\beta e^{-\xi\omega_0 t} \left[ \sin \varphi \cos \omega_d t + \frac{\omega_0}{\omega_d} (\xi \sin \varphi - s \cos \varphi) \sin \omega_d t \right] \\ z_3(t) = B\beta \sin(\omega t - \varphi) \end{cases} \quad (2)$$

$$\begin{cases} \omega_d = \omega_0 \sqrt{1 - \xi^2} \\ s = \frac{\omega}{\omega_0} \\ B = \frac{F_0}{K} \\ \beta = \frac{1}{\sqrt{(1-s^2)^2 + (2\xi s)^2}} \\ \varphi = \tan^{-1} \frac{2\xi s}{1-s^2} \end{cases} \quad (3)$$



where  $\omega_0$  and  $\omega_d$  are the resonant frequencies, with  $\omega_d$  representing the damped resonant frequency.  $\xi$ ,  $B$ , and  $\varphi$  are the damping ratio, static displacement, and phase angle of the PMUT, respectively.

The displacement  $z(t)$  of the PMUT is composed of two parts: the free vibration response  $z_1(t)$  and forced vibration response  $z_2(t) + z_3(t)$ ;  $z_1(t)$  is related to the initial condition of the PMUT,  $z_2(t)$  represents the transitional phase of forced vibration, which gradually decays to 0 due to damping, and  $z_3(t)$  represents the steady-state of forced vibration.

The static displacement  $B$  and the resonant frequency  $\omega_0$  of the composite triangular cantilever beam as shown in Fig. 1c, are given by<sup>21,24</sup>:

$$B(x) = \frac{6e_{31}h_e U}{K_A} x^2 \quad (4)$$

$$\omega_0 = \frac{4.14}{L^2} \sqrt{\frac{E_1(H_1 - Z_n)^3 + E_1 Z_n^3 + E_2(H_1 + H_2 - Z_n)^3 - E_2(H_1 - Z_n)^3}{\rho_1 H_1 + \rho_2 H_2}} \quad (5)$$

$$\begin{cases} K_A = \sum_i E_i (H_i^3 + 12H_i(z_i - Z_n)^2) \\ h_e = \frac{H_2}{2} + H_1 - Z_n \\ Z_n = \frac{\sum_i E_i z_i H_i}{\sum_i E_i H_i} \end{cases} \quad (6)$$

where  $e_{31}$  is the piezoelectric coefficient of the piezoelectric layer,  $U$  is the driving voltage.  $E_i$ ,  $\rho_i$ ,  $H_i$  and  $z_i$  represent the Young's modulus, density, thickness, and mid-plane position of the  $i$ th layer, respectively.

When the device operates at the resonant frequency starting from a zero initial state, the displacement of the PMUT can be simplified as:

$$z(t) = QB \left( 1 - e^{-\frac{\omega_0 t}{2Q}} \right) \sin \left( \omega_0 t - \frac{\pi}{2} \right) \quad (7)$$

where  $Q$  represents the quality factor of the PMUT, governing both its amplitude rise rate and steady-state amplitude.

After removing the excitation, the forced vibration terms  $z_2(t)$  and  $z_3(t)$  become zero and the PMUT falls into residual vibration stage, where its displacement can be expressed as:

$$z(t) = QB e^{-\frac{\omega_0 t}{2Q}} \cos \omega_0 t \quad (8)$$

At this time, its displacement will decay exponentially, with the decay rate determined by the quality factor  $Q$  and further influenced by the mode damping. When PMUT operates in the synchronous vibration mode, it can be equivalently represented as a vibrating piston with an area

of  $S_{\text{eff}}$ , and its acoustic radiation damping  $R_r$  is<sup>25,26</sup>:

$$\begin{cases} R_r = \frac{\rho_0 c_0 k^2}{2\pi} S_{\text{eff}}^2 \\ S_{\text{eff}} \approx 0.17 S_{\text{PMUT}} \end{cases} \quad (9)$$

where  $\rho_0$ ,  $c_0$ ,  $k$ , and  $S_{\text{PMUT}}$  represent the sound speed, air density, wave number, and the area of the proposed PMUT, respectively.

Due to the resonant frequency of the cantilever beam is dependent on its length and the thickness of each layer in the stack according to Eq. (5), any dimension deviation induced by process can lead to resonant frequency change. If the resonant frequencies of the PMUT cantilever beams are inconsistent, asynchronous vibration will happen. When adjacent cantilever beams oscillate out of phase with equal amplitude, they can be regarded as a pair of acoustic dipoles. In this condition, the radiation damping of the asynchronous vibration mode  $R_r'$  can be calculated as<sup>26</sup>:

$$R_r' = \frac{\rho_0 c_0}{6\pi} k^4 l^2 S_{\text{eff}}^2 \quad (10)$$

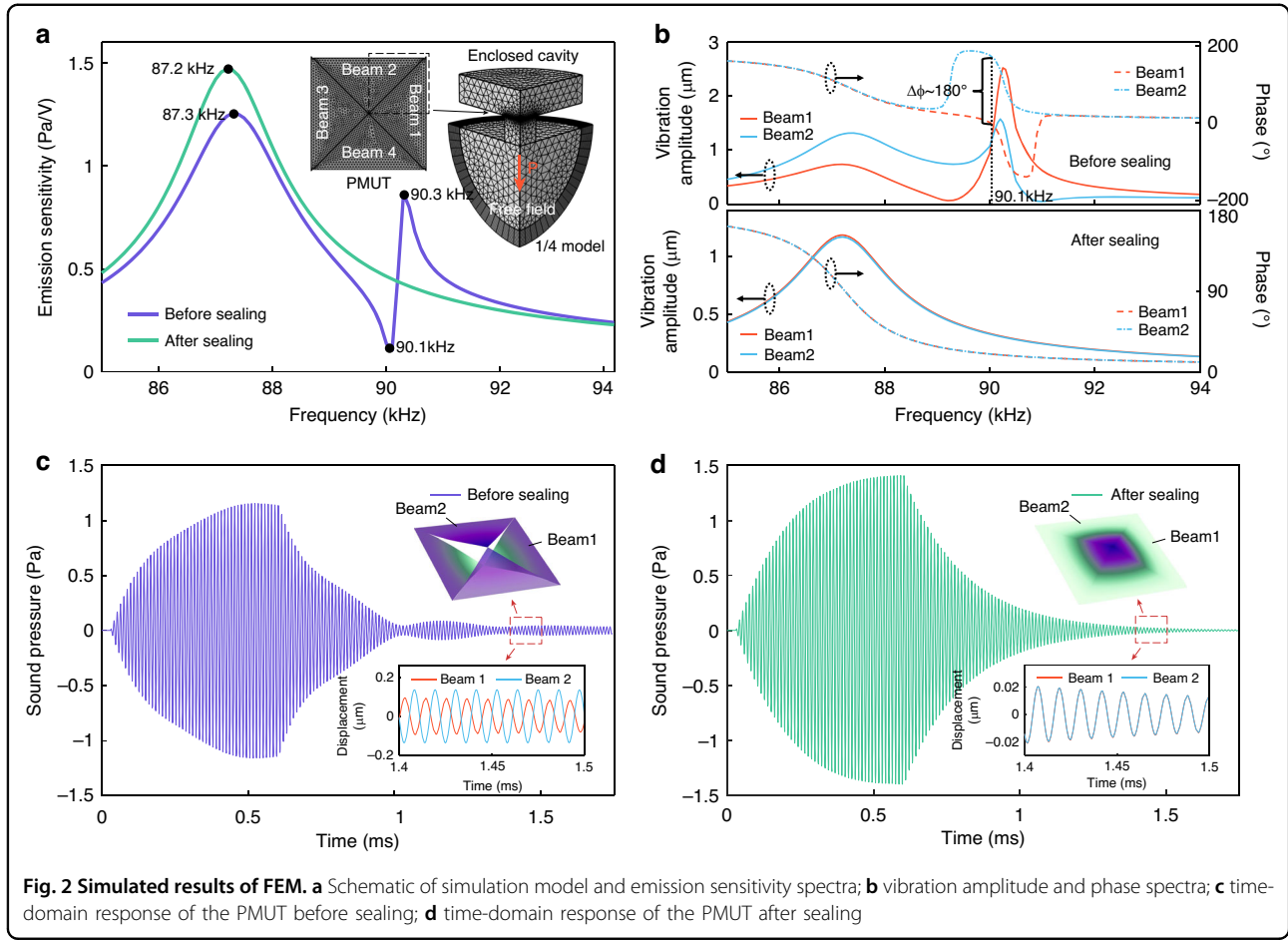
where  $l$  represents the spacing between adjacent cantilever beams.

Combining Eqs. (9) and (10), the ratio of asynchronous vibration damping to synchronous vibration damping can be determined as follows:

$$\frac{R_r'}{R_r} = \frac{k^2 l^2}{3} \quad (11)$$

By substituting corresponding values ( $f_0 = 87.3$  kHz, based on the simulation results in Fig. 2a;  $l = 339.4$   $\mu\text{m}$ , which is the centroid spacing between adjacent cantilever beams) into equation,  $\frac{R_r'}{R_r} \approx 0.098$  can be obtained, indicating that the radiation damping under the asynchronous vibration is far smaller than that of the synchronous one. According to Eq. (8), when the PMUT operates in synchronous vibration mode, its ring-down time (the time taken for the displacement to decay to approximately 5% of the steady-state amplitude) can be calculated by the product of the quality factor  $Q$  and the vibration period. In contrast, due to the significantly lower radiation damping associated with the asynchronous vibration, the ring-down time will be prolonged, resulting in an extended blind area.

In the current case, the PDMS is used to seal the air gaps in the PMUT, thereby constructing a soft inter-connecting spring between adjacent cantilever beams to suppress the asynchronous vibration and reduce the blind area as well. During the sealing process, the liquid PDMS will be spontaneously driven to fill the gaps by the capillary force if the condition for spontaneous capillary



flow (SCF) is met<sup>27</sup>:

$$\frac{G}{H} < \cos(\Omega) \quad (12)$$

where  $G$  and  $H$  represent the gap width and the cantilever beam thickness, respectively.  $\Omega \approx 23^\circ$  is the contact angle between the liquid PDMS and the Si sidewall surface<sup>21</sup>.

The cured PDMS forms a soft spring between the cantilever beams as shown in Fig. 1b. Under the action of shear forces  $\tau S$ , the PDMS spring undergoes a deformation  $z$ , and the shear stiffness of the spring is calculated by:

$$k_t = \frac{\tau S}{z} = \left( T \cdot \frac{z}{G} \right) \cdot \left( \sqrt{2} L \cdot H \right) \frac{1}{z} = 192.2 \text{ N/m} \quad (13)$$

where  $T = 251.7 \text{ kPa}$  is the shear modulus of PDMS.

At the same time, the equivalent stiffness of the triangular cantilever beam is calculated by:

$$k_r = \frac{K_A W}{6L^3} = 38.1 \text{ N/m} \quad (14)$$

It can be found that the shear stiffness of the PDMS spring is approximately five times that of the cantilever beam. As a result, it can provide sufficient strength to effectively suppress the asynchronous vibration between adjacent cantilever beams and force them to vibrate in synchronous mode.

After sealing, the proposed cantilever beam-based PMUT will operate in the synchronous vibration mode. Based on the far-field sound pressure formula for a piston on an infinite baffle, the sound field distribution of the proposed PMUT is given by<sup>2,26</sup>:

$$\begin{cases} p(d, \theta, t) = p_d(d, t) \cdot D(\theta) \\ p_d(d, t) = 0.34 \pi \rho_0 S_{\text{PMUT}} w f^2 g \frac{10^{-\alpha d}}{d} e^{j(\omega t - kd)} \\ D(\theta) = \frac{2J_1(ka \sin(\theta))}{ka \sin(\theta)} \end{cases} \quad (15)$$

where  $d$  represents the sound propagation distance;  $a$ ,  $w$ ,  $f$  and  $g$  represent the equivalent piston radius, vibration amplitude, operating frequency and back cavity gain of PMUT, respectively.  $\alpha$  is the sound absorption coefficient of the air medium, which is related to the sound frequency, ambient atmospheric pressure, temperature



and humidity.  $J_1$  is the first-order Bessel function.  $p_d(d, t)$  and  $D(\theta)$  represent the axial distribution and the angular distribution of sound pressure, respectively.

The equivalent piston radius  $a$  of the currently designed cantilever beam-based PMUT is calculated to be 167.8  $\mu\text{m}$  according to Eq. (9). Consequently, the condition  $ka = 0.27 < 1$  is satisfied, allowing for the calculation of  $D(\theta) \approx 1$ , which demonstrates the omnidirectional sound field distribution. In addition, the emitted sound pressure  $p_d(d, t)$  decreases with distance. At the short distance, the emitted sound pressure is approximately inversely proportional to distance. With the increasing propagation distance, the sound absorption loss will become dominant, thereby affecting the maximum detection range of the PMUT rangefinder.

As the increasing target distance, the amplitude of the pulse-echo signal received by the PMUT rangefinder will gradually decrease until it approaches to the detection threshold. At this point, the random thermal noise might induce false identification for the target signal, the average time of which is given by<sup>8</sup>:

$$t_{fa} = \frac{1}{BW} e^{\frac{V_{TH}^2}{\delta_A^2}} \quad (16)$$

where  $BW$  is the PMUT operation bandwidth,  $\delta_A$  is the root mean square (RMS) noise.  $V_{TH}$  is the threshold voltage and it must be significantly higher than the system's noise level to ensure accurate target identification.

Finite element simulation is conducted using COMSOL Multiphysics 6.0, and the simulation model is schematically shown in the inset of Fig. 2a. To simulate asynchronous vibration mode, the lengths of the cantilever beams 2 and 4 are intentionally set to be 359  $\mu\text{m}$ , which is 1  $\mu\text{m}$  shorter than those of the cantilever beams 1 and 3. The remaining structure parameters of the PMUT are consistent with the design specifications. The back side of the PMUT is used for sound emission and reception, while its front side is enclosed by a cylindrical cavity to prevent acoustic interference. The emission sensitivity spectra of the proposed PMUT, both before and after PDMS sealing, are obtained at an axial distance of 10 mm using the "External Field Calculation" function, as shown in Fig. 2a. Before sealing, the PMUT exhibits a bit more complicated frequency response, in which a resonance peak at 87.3 kHz with emission sensitivity of 1.25 Pa/V can be observed. At the same time, a distinct dip around 90.1 kHz and a second peak around 90.3 kHz can also be found, which are thought to be mainly caused by the asynchronous vibration between these cantilever beams. In comparison, after sealing, a normal frequency response can be obtained, where it demonstrates only one single resonance peak at 87.2 kHz with slightly higher emission sensitivity of 1.47 Pa/V. It is believed that the four

cantilever beams will be forced to vibrate synchronously as a whole under the connection effect of the PDMS. In order to further validate the mechanism behind these phenomena, the changes of the vibration amplitude and the phase of these two sets of cantilever beams with respect to the frequency are also studied. From the results shown in Fig. 2b, it can be seen that as for the PMUT before sealing, all of the cantilever beams will vibrate synchronously before reaching to the first-order resonant frequency. Then, with continuous increase of the frequency, both of the vibration amplitudes and phases of these cantilever beams will gradually change, leading to the generation of the asynchronous vibration mode. In particular, at the frequency of 90.1 kHz, the phase difference between the cantilever beams 1/3 and 2/4 becomes close to 180°, and they demonstrate the same vibration amplitude. As a result, their generated sound pressures will be largely canceled out by each other, leading to an abrupt drop in the emission sensitivity. In comparison, at the frequency of 90.3 kHz, although the phase difference is still about 180°, the vibration amplitude of the cantilever beams 1/3 is significantly larger than those of the cantilever beams 2/4, resulting in a net sound pressure output peak. After that, with the further increasing frequency, all of the cantilever beams will return to the synchronous vibration state. This complex response is caused by the mutual coupling between these two sets of cantilever beams. In contrast, after sealing, both of the vibration amplitudes and phases of these cantilever beams will align well with each other, verifying the expected synchronous vibration as a whole.

To further investigate the time-domain response of the PMUT before and after sealing, a 2  $V_{pp}$ , 50 cycles sinusoidal signal is used to drive the PMUT, with driving frequencies of 87.3 kHz and 87.2 kHz, respectively. According to Eqs. (2) to (5), the cantilever displacement is determined by the forced and the free oscillations, which are influenced by both of the driving signal and the synchronous/asynchronous vibration modes of the PMUT. The emitted sound pressures at an axial distance of 10 mm of the PMUT before and after sealing are shown in Fig. 2c, d, respectively. It can be found that in both cases, the amplitude of the emitted sound signal will increase according Eq. (7) at the initial stage and gradually reach a steady state after 50 cycles driving pulses. Once the driving signal is removed, the PMUT will enter into the ring-down stage, in which the residual displacement of PMUT cantilevers as well as the generated sound pressure will be governed by their resonant mode instead. As for the PMUT before sealing, the vibration displacement changes of the cantilever beam 1 and 2 within the time range from 1.4 ms to 1.5 ms are especially extracted out as shown in Fig. 2c, from which out-of-phase vibration between them can be clearly observed, validating the

appearance of asynchronous vibration phenomenon. Due to the associated lower radiation damping, the residual sound pressure amplitude of the PMUT demonstrates a complicated oscillation-like decay tendency, resulting in a longer ring-down tail. In contrast, after PDMS sealing, the asynchronous vibration between the PMUT beams can be effectively suppressed. As comparison, the vibration displacement changes of the cantilever beam 1 and 2 within the same time range are also provided as shown in Fig. 2d. It is observed that they vibrate in perfect synchronization with displacement amplitude significantly lower than that of the same device before sealing. As a result, upon removal of the driving pulse, the sound pressure amplitude decreases rapidly in exponential form, with its decay rate determined by the quality factor  $Q$ .

### Fabrication

The fabrication process flow of the proposed PMUT is shown in Fig. 3a. It starts with a commercial SOI wafer with 3  $\mu\text{m}$ -thick silicon device layer, 1  $\mu\text{m}$ -thick buried oxide layer and 720  $\mu\text{m}$ -thick silicon handle layer. Firstly, the stack structure including the bottom electrode layer (Mo), the piezoelectric layer (AlN) and the top electrode layer (Mo) are deposited onto the device layer using sputtering method, with their thicknesses of 0.2  $\mu\text{m}$ , 1  $\mu\text{m}$ , and 0.2  $\mu\text{m}$ , respectively. Subsequently, the layers of top Mo, AlN, and bottom Mo are sequentially patterned using a combination of photolithography and reactive ion etching (RIE) techniques. A 0.2  $\mu\text{m}$ -thick  $\text{Si}_3\text{N}_4$  film that serves as an electrical insulation layer is subsequently deposited onto the wafer surface via plasma-enhanced chemical vapor deposition (PECVD) followed by dry etching to create both of the electrical connection vias for the metal layer and the etching windows for the air gaps and the liquid reservoirs. After that, an aluminum film is deposited via sputtering and patterned to create the metal wirings for the top and bottom Mo electrodes and the bonding pads for packaging, during which to ensure good step coverage, its thickness is selected to be 0.5  $\mu\text{m}$ . The front side process ends with the patterning of the silicon device layer using DRIE to create the air gaps and the reservoir structures. Then, the handle layer of the SOI wafer is ground and polished to a desired thickness of around 450  $\mu\text{m}$  to facilitate the etching of the back cavity in a subsequent step. The thinned substrate is selectively etched by DRIE to form the back cavity, and the shape and size of the back cavity determine the overall geometry of the PMUT, which in turn governs the mechanical performance of the cantilever beams. In this step, double-sides photolithography alignment, the sidewall angle of the back cavity, and the imperfect etching of right angles may introduce dimension deviations, leading to inconsistent dimensions of the cantilever beams in the PMUT. Then, the exposed buried oxide layer is removed using vapor HF

to release the PMUT structure. After the release step, the whole wafer is laser diced into individual dies for subsequent wire bonding and testing. The post-processing PDMS sealing treatment is ultimately applied to form soft connections between the cantilever beams, which follows our previous method. The PMUT device is fixed onto the microscope objective table and the dispensing needle is moved above its reservoir region through a three-axis positioning stage. PDMS droplet with standard mixing ratio (the PDMS base and the curing agent with a weight ratio of 10:1) is injected into the reservoir and its amount is precisely controlled using a commercial dispenser (SUPER  $\Sigma\text{CMII V5}$ , Musashi, Japan). Under the capillary effect, the liquid PDMS will flow into the gap spontaneously by the surface tension. After filling, the device is placed into an oven for complete curing.

The as-fabricated device structure is firstly checked using SEM as shown in Fig. 3b, from which the four triangular cantilever beams, the air gaps between them, the metal bonding pads and the reservoirs can be clearly observed. At the same time, the white light profilometer is used to measure the surface contour of the as-fabricated structures. From the results shown in Fig. 3c, it can be seen that all of the four cantilever beams deflect upward, demonstrating the existence of residual tensile stress in the deposited stack layer. This initial warpage will slightly widen the gap, especially at the tip region of the cantilevers, where the gap width is measured to be 2.2  $\mu\text{m}$ . The cross-section of the as-deposited  $\text{Si}_3\text{N}_4/\text{Mo}/\text{AlN}/\text{Mo}$  layers is observed by combining focused ion beam (FIB) with SEM, from which their thicknesses are measured to be 229 nm/189 nm/1043 nm/182 nm, respectively, agreeing with the design specifications. In addition, the thickness of the silicon device layer is measured to be 2.6  $\mu\text{m}$ , which is a bit smaller than the design value due to the thickness variation tolerance of the currently used commercial SOI product, leading to a decrease in the resonant frequency of the fabricated device. Based on this thickness, the SCF condition for PDMS liquid filling can be satisfied when the gap widths are less than 2.39  $\mu\text{m}$ , confirming that the current device meets this requirement for spontaneous capillary filling. Figure 3d, e shows the SEM images of the cantilever tip regions before and after PDMS sealing, respectively. It can be found that most of the gaps are well sealed by PDMS except for the vertex region with relatively large gap size, which breaks the SCF condition and the automatic filling cannot be achieved. Since the unsealed area is very small (4  $\mu\text{m} \times 4 \mu\text{m}$ ), its impact on the shear stiffness of the PDMS spring is negligible. Therefore, this method can effectively suppress the asynchronous vibration of the PMUT. In addition, since the PMUT operates at relatively high frequency, the impact of the air leakage through the unsealed region on its acoustic performance should be minimal.

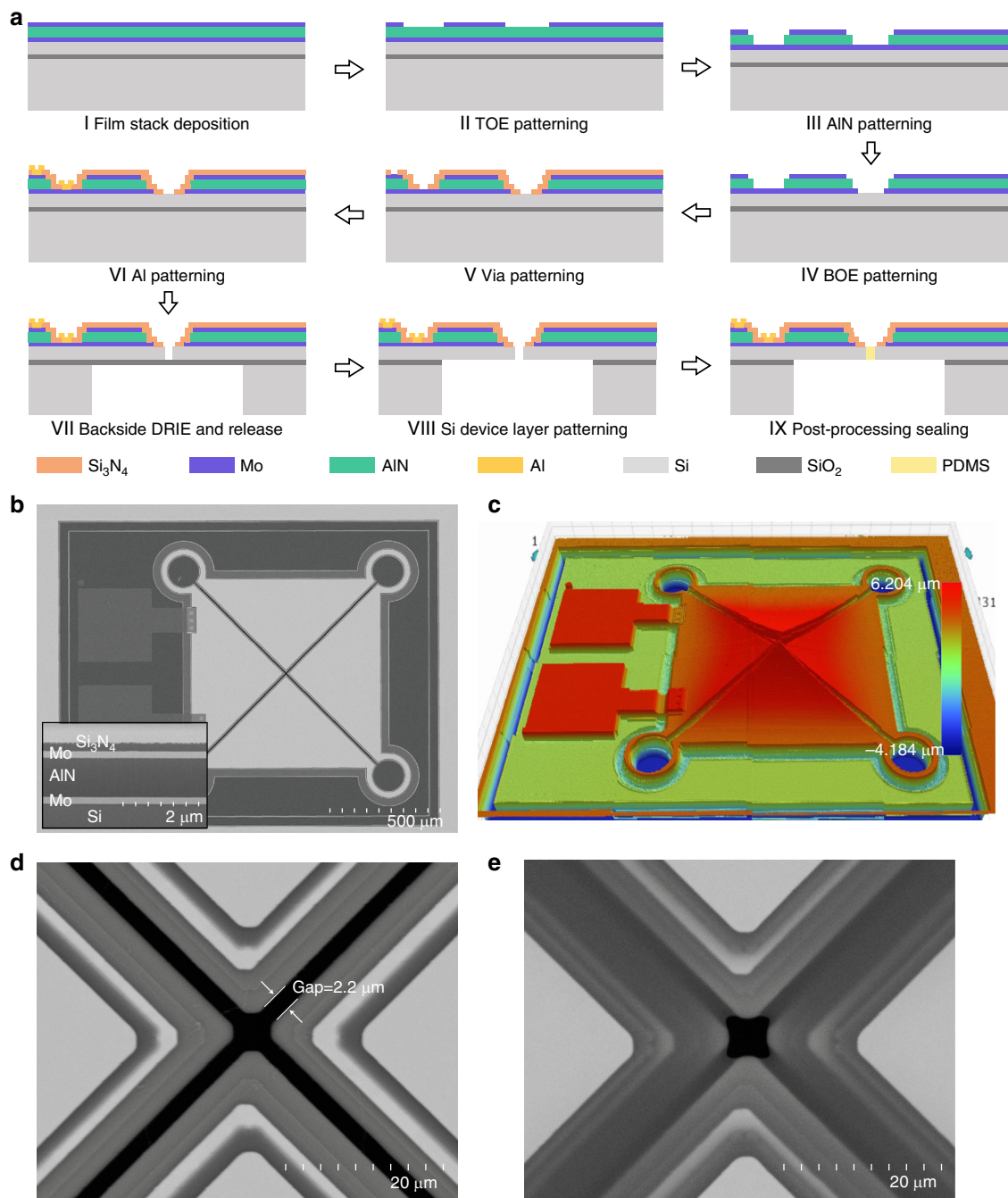


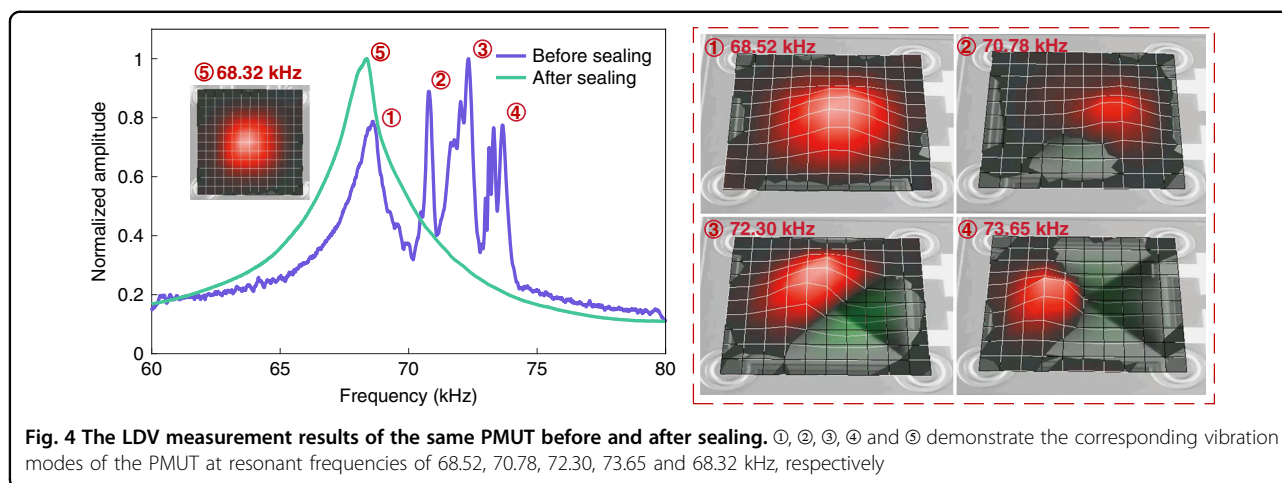
**Fig. 3** The fabrication results of the PMUT. **a** Schematic of the fabrication process flow of PMUT; **b** SEM of the fabricated device; **c** surface profile of the fabricated device; **d** SEM image of the tip region of the PMUT before sealing; **e** SEM image of the tip region of the PMUT after sealing

## Results

To characterize the mechanical response of the device, a laser Doppler vibrometer (LDV, MSA 600, Polytec, Germany) is used to measure the displacement spectra and the vibration modes of the PMUT before and after sealing as shown in Fig. 4. During the measurement, the PMUT is held with both of its front and back sides open to the air.

Due to the inconsistent size of each cantilever beam and the mechanical cross-talk between them, the displacement of the PMUT before sealing demonstrates multiple resonance peaks within frequency range from 68.52 kHz to 73.65 kHz. The four main vibration modes are extracted out and marked as ①, ②, ③ and ④, respectively. At 68.52 kHz, all four cantilevers vibrate synchronously.





With the increasing driving frequency beyond each resonant frequency, the response phase of these beams will be reversed sequentially, resulting in the different asynchronous vibration modes as shown in ②, ③ and ④. After sealing, the resonance peaks will be merged into one at a frequency of 68.32 kHz, exhibiting synchronous vibration mode as illustrated in ⑤. The  $Q$  value of the PMUT after sealing is measured to be 39.1. Obviously, the LDV measurement results validate that the sealing treatment can effectively suppress the asynchronous vibration modes of the cantilever beam-based PMUT and demonstrates little impact on its original performance.

To characterize the acoustic performance of the device, an optical microphone (Eta250 Ultra, XARION, Austria) that is placed at an axial distance of 100 mm is used to measure the sound pressure spectra generated by the PMUT before and after sealing, as shown in Fig. 5a. During the measurement, the front side of the PMUT is covered by an enclosed cavity to avoid acoustic interference from opposite transmission and all of the cantilever beams are driven with the same  $10 V_{pp}$  continuous sinusoidal signal with its frequency being swept from 67 kHz to 76 kHz. As for the PMUT before sealing, due to the resonant frequency difference, these cantilever beams will undergo vibration transition from synchronous mode to asynchronous one as revealed by LDV measurement. As a result, their generated sound pressures will be partially canceled out by each other and demonstrate a distinct pressure drop within the frequency band between 70 kHz and 73 kHz. In contrast, under the effect of the forced synchronous vibration after sealing treatment, only a single resonance peak at 69.2 kHz can be found in the sound pressure frequency spectrum.

To further assess the effect of the sealing on the PMUT working performance, the changes of the sound pressure with the driving voltage at the resonant frequency (69.5 kHz for the unsealed PMUT and 69.2 kHz for the

sealed PMUT) are studied as shown in Fig. 5b. When the driving voltage is below  $25 V_{pp}$ , the sound pressure generated by the sealed PMUT is slightly larger than that of the unsealed one due to the reduced thermal viscous damping occurring at the air gap, demonstrating higher emission sensitivity. As the increasing driving voltage, the PMUT displacement will also increase. However, for both unsealed and sealed PMUTs, significant deformation will lead to the stress stiffening effect, pushing the PMUT into a nonlinear regime where the emission sensitivity will be gradually decreased. Moreover, as for the sealed PMUT, the PDMS in the gap will apply additional tensile stress onto the cantilever beams, thus limiting further displacement and resulting in lower sound pressure.

At the same time, the emitted sound pressure waveforms from the PMUTs before and after sealing in the time domain are also recorded as shown in Fig. 5c, d, respectively. Here, the PMUTs are driven under their resonant frequencies by a  $10 V_{pp}$ , 30-cycle sinusoidal signal instead. After removing the excitation signal, both of the sound pressure waveforms exhibit obvious ring-down phenomenon but the details are quite different. In the case of the unsealed PMUT, a significantly prolonged oscillation-like ring-down tail can be found mainly due to the occurrence of the asynchronous vibration, which can severely interfere with the reception of the echo signal in time-of-flight (ToF) rangefinder applications. After sealing, since the forced synchronous vibration can provide greater radiation damping, faster decay rate and shorter ring-down time can be obtained. According to previous theoretical analysis, the  $Q$  value of the sealed PMUT can be calculated to be 43.2 by exponential fitting to the decay data according to Eq. (8). The slightly higher resonant frequency and quality factor  $Q$  than the LDV measurement results are primarily due to the reduced radiated mass as well as radiation damping caused by the enclosed

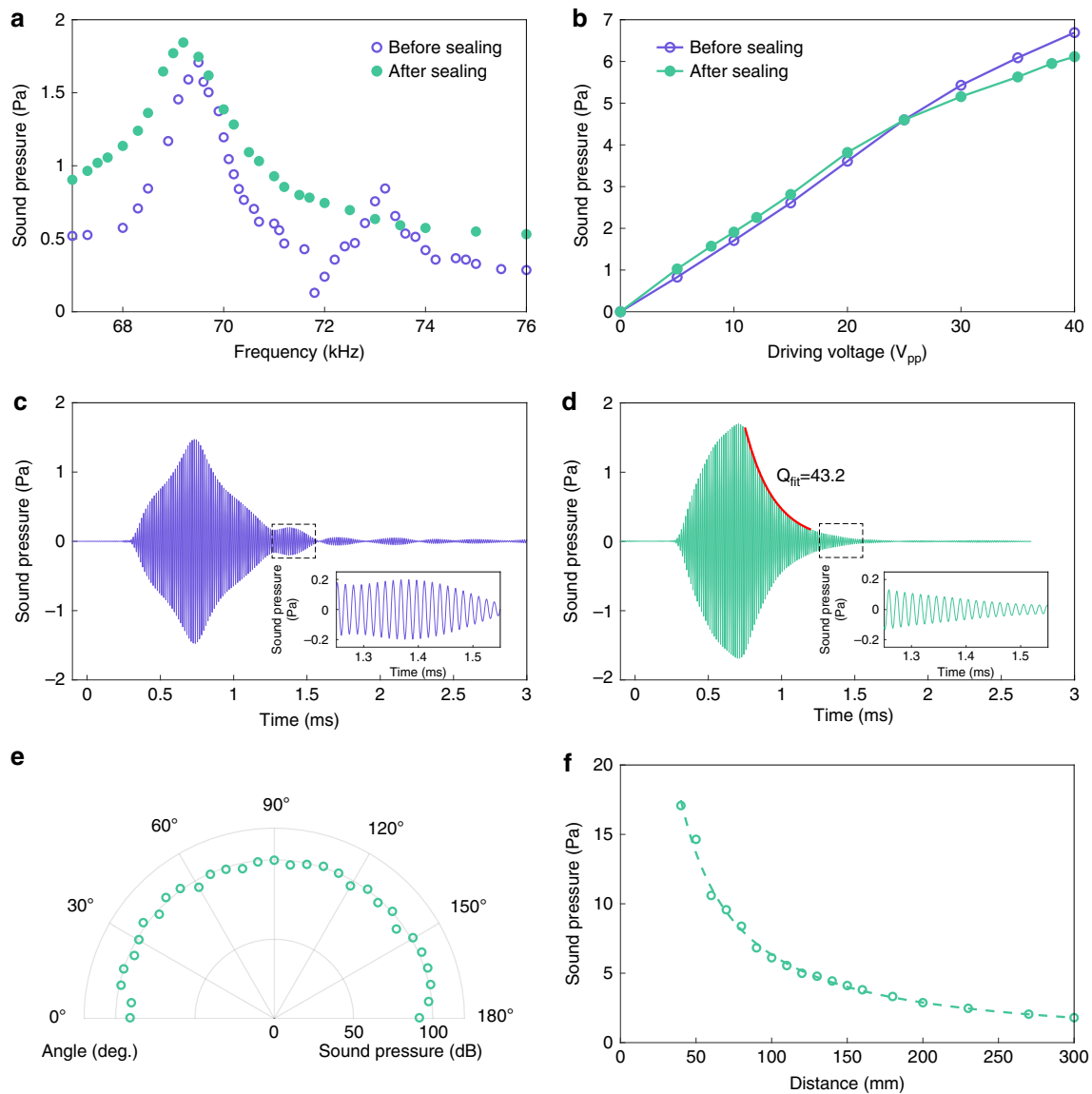


**Fig. 5 PMUT emission sound pressure measurement results.** **a** Sound pressure frequency spectra; **b** relationship between sound pressure and driving voltage; **c** time-domain response of sound pressure before sealing; **d** time-domain response of sound pressure after sealing; **e** relationship between sound pressure and angle, with a driving voltage of  $10 V_{pp}$  at a measurement distance of 100 mm; **f** relationship between axial sound pressure and distance, with a driving voltage of  $40 V_{pp}$

front cavity. It's obvious that both of the frequency and time domain measurement results agree well with those of the simulation, validating the effectiveness of the proposed method.

Figure 5e, f provides the angular and axial sound pressure distribution of the PMUT after sealing, respectively. From which, a  $-6$  dB divergent angle is measured to be approximately  $170^\circ$ , demonstrating nearly omnidirectional radiation characteristics. Moreover, like theoretical estimation, a monotonous decrease of the emitted sound pressure with the increasing transmission distance can also be found.

Based on the sealed PMUT, a self-transceiving range measurement setup is built as shown in Fig. 6. In experiment, a front-end circuit incorporating transmission/reception switching, signal amplification and band-pass filtering functions is designed for current PMUT. Two output channels of the function generator are used to provide a chopped sinusoidal signal for driving the PMUT and a logic pulse signal for controlling the switch, respectively. In the beginning, the PMUT works under the transmission mode, during which the driving signal is amplified by an operational amplifier (OPA) and then applied to the PMUT. After that, the front-end circuit will

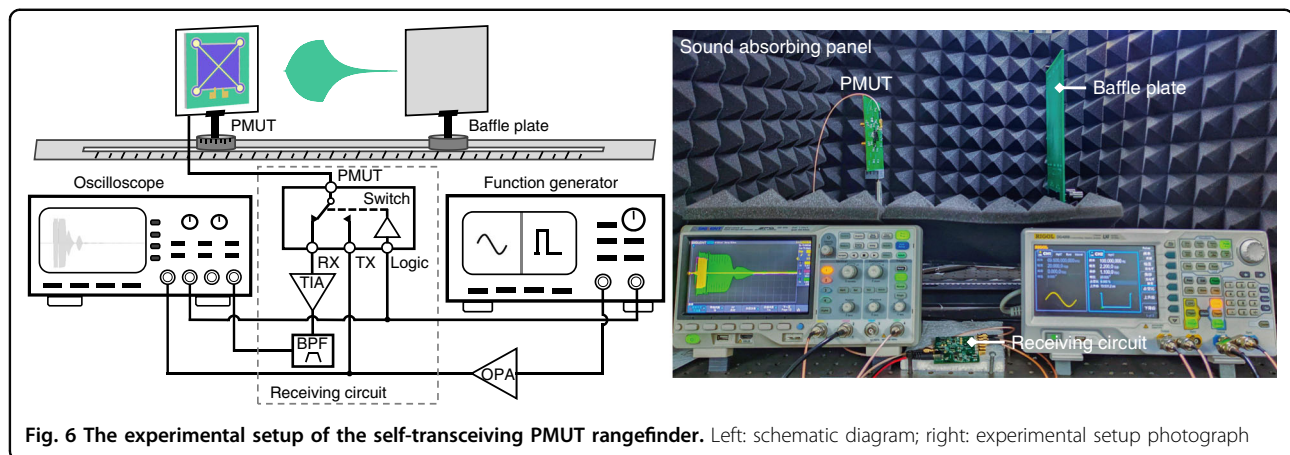


**Fig. 6** The experimental setup of the self-transceiving PMUT rangefinder. Left: schematic diagram; right: experimental setup photograph

be switched to the reception mode, where the charge signal from the PMUT will be firstly translated into an amplified voltage signal by a transimpedance amplifier (TIA) and subsequently processed by a bandpass filter (BPF) before being recorded by an oscilloscope. Through measuring the time of flight of the pulse-echo signal, the distance information can be obtained. A baffle plate is used as the target and its distance to the PMUT can be adjusted using a sliding rail. To avoid interference from stray reflected waves, the experimental setup is surrounded by the sound absorbing panel.

During the experiment, both of the PMUTs before and after sealing are driven under their resonant frequencies by a 40 V<sub>pp</sub>, 50 cycles sinusoidal signal, and the pulse width of the switch signal is set to be slightly longer than the driving signal. Their output signals from the receiving circuit in the absence of a target object are firstly characterized as shown in Fig. 7a, b, respectively. Initially, the switch signal is set at a high logic level of 2.2 V to make the PMUT operate in the transmission mode. In this stage, due to the incomplete electromagnetic isolation of the switch and the high sensitivity of the charge amplifier, some output coupling signals from the receiving circuit still can be found. Then, the switch signal is translated to a low logic level and the PMUT will be changed into reception mode. During this period, the PMUT will experience residual vibration after the driving signal is removed, with gradually decayed amplitude over time. The charges from the PMUT induced by the residual vibration will be processed by the receiving circuit, and generate corresponding output signal, from which the residual vibration status of the PMUT can be revealed. In the unsealed case, an oscillation like ring-down output signal with larger amplitude and significantly prolonged tail can be observed, representing the presence of the asynchronous vibration as mentioned before. Considering the following echo signal detection requirement, this will

lead to a blind area greater than 1 m. In contrast, after sealing, the residual vibration signal is distinctly shortened. By fitting the envelope of the residual vibration signal, the *Q* value of the PMUT is calculated to be 40.4, which is close to the results from the LDV and the sound pressure measurements.

The range measurement performance of the sealed PMUT is characterized as illustrated in Fig. 7c, d, which present the blind area and the maximum detection distance results, respectively. In the blind area measurement experiment, with the baffle plate being moved close to the PMUT, the echo signal will shift toward the residual vibration signal of the PMUT and merge with it. As the barrier continues to approach, the waveform of the merged echo signal will fluctuate, thus affecting the peak detection for the echo signal. From the experiment, it can be found that when the ratio of the peak amplitude of the echo signal to that of the ring-down signal is larger than 2, the echo signal peak can be identified accurately as shown in Fig. 7c. The peak detection algorithm identifies multiple echo signals, with the nearest first echo signal representing the baffle, while the remaining signals are due to multiple reflections between the PMUT and the baffle. Consequently, the blind area of the developed PMUT rangefinder is calculated to be 270.8 mm.

In the maximum distance detection experiment, a movable rectangle baffle with a size of 1 m × 1.5 m is used as the reflective object instead. With the baffle plate being moved away from the PMUT, the amplitude of the echo signal will decrease, as shown in Fig. 7d. The relationship between the SNR of the echo signal and the distance is fitted using Eq. (15), as indicated by the green curve in the figure. To determine the maximum detection distance of the PMUT rangefinder, a threshold detection algorithm is employed by comparing the SNR to a predetermined threshold. The minimum detectable SNR is calculated to be 11.5 dB using Eq. (16) so as to ensure that the average

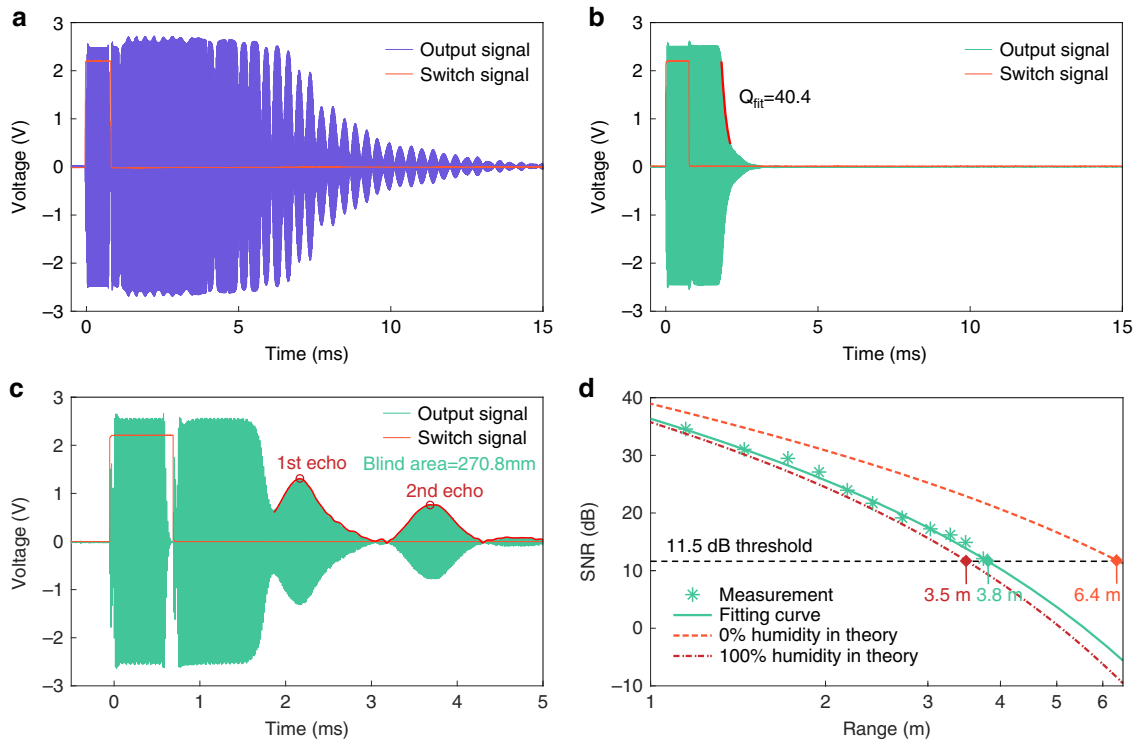


**Fig. 7** The ring-down signal and range measurement of PMUT. **a** The ring-down signal before sealing; **b** The ring-down signal after sealing; **c** Blind area measurement results of the PMUT after sealing, with a driving signal of  $20 V_{pp}$ -40 cycles sinusoidal pluses; **d** Maximum distance measurement results of the PMUT after sealing, with a driving signal of  $40 V_{pp}$ -40 cycles sinusoidal signal

occurrence time of false alarms exceeds 30 minutes. Based on the intersection of the SNR fitting curve and the threshold, the maximum detection distance of the sealed PMUT is determined to be 3.8 m.

Variations in the working environment can lead to alterations in acoustic absorption loss coefficients and sound velocity thereby affecting the performance of PMUT-based rangefinders. The acoustic absorption loss coefficient is influenced by multiple environmental factors, including air humidity, temperature, and atmospheric pressure, with humidity having a particularly significant impact. In the current laboratory testing environment, the ambient temperature and humidity are recorded to be  $20^{\circ}\text{C}$  and 50%, respectively. According to theoretical formulas<sup>28</sup>, the relationships between SNR and distance under 100% and 0% humidity are also calculated, yielding corresponding maximum detection distances of 3.5 m (100% humidity) and 6.4 m (0% humidity), respectively. The sound velocity is primarily dependent on the ambient temperature, and its relationship can be quantitatively described by Eq. (17), where  $T$  represents the temperature in  $^{\circ}\text{C}$ <sup>29</sup>. To address this issue, a temperature measurement module can be integrated into the rangefinder system to monitor the ambient temperature in real time and correct the sound velocity, thereby enhancing

the ranging accuracy<sup>30</sup>.

$$c(T) \approx 331\text{m/s} + 0.6 \frac{\text{m/s}}{^{\circ}\text{C}} \cdot T \quad (17)$$

A performance comparison between the proposed PMUT and the state-of-the-art AIN PMUT-based in-air rangefinders is provided in Table 1. For rangefinders operating in non-pulse-echo mode, their maximum detection distance is obtained by dividing the ultrasonic wave traveling distance by two. From the structural perspective, the quasi-closed structure adopted in ref. <sup>16</sup>, partially relieves stress through its open design, but the mechanical connections in the driving region limit complete stress release, resulting in significant resonant frequency shifts due to accumulated residual stress from the fabrication process. Reference <sup>10</sup> employs a fully-closed diaphragm structure, which exhibits higher stress sensitivity than the quasi-closed design, leading to more severe resonant frequency shifts; moreover, its limited linear operating range significantly restricts the displacement and acoustic emission performance of the device. Reference <sup>31</sup> also utilizes a fully-closed diaphragm structure and, in addition to the aforementioned drawbacks, requires additional PMUT units due to its separate-



**Table 1** Performance comparison of the state-of-the-art AlN PMUT-based in-air rangefinders

Resonant frequency	Piezoelectric material	Working mode	Element number	Diaphragm area	Distance detection range	Reference
69.2 kHz	AlN	Self-transceiving	1	0.518 mm <sup>2</sup>	270.8 mm–3.8 m	This work
71.5 kHz	AlN	Self-transceiving	1	0.59 mm <sup>2</sup>	170.7 mm–3.0 m	Ref. <sup>16*</sup>
76.4 kHz	AlN	Self-transceiving	1	1.77 mm <sup>2</sup>	300 mm–1.5 m	Ref. <sup>10</sup>
29 kHz	AlN	Separate-transceiving	2	5.29 mm <sup>2</sup>	400 mm**–1.4 m	Ref. <sup>31</sup>

\*The previous work of our team  
\*\*The blind area results from cross-talk between the TX and RX PMUTs

transceiving mode, as well as facing frequency matching issues between the transmitting and receiving units. From the detection performance perspective, compared to other state-of-the-art PMUTs, the proposed PMUT can provide the largest range of distance detection capability with the smallest device diaphragm area. Moreover, through combining strategies such as reducing the cycles of driving pulses and using phase-shifted driving<sup>32</sup>, the blind area can be shorten, increasing the detection range further.

Discussion and conclusions

This work proposes a novel cantilever-beam based PMUT with specifically designed reservoir structures, where the liquid PDMS can be applied to spontaneously seal the air gaps between the already released cantilever beams through the capillary effect. The cured PDMS will serve as soft spring connecting the adjacent cantilever beams to suppress their asynchronous vibration. The effectiveness of this post processing strategy is firstly studied by theoretical analysis and finite element simulation, and subsequently validated by the mechanical and acoustic response measurement results. At the same time, through performance comparison to the state-of-the-art counterparts, the largest range detection capability has been successfully demonstrated in experiment, although the effective diaphragm area of the current PMUT is the smallest. Provided the simple treatment process and significant performance improvement effectiveness, the same strategy can also be used to develop ultrasonic sensor arrays to further enhance the rangefinder performance and enable expanded applications such as gesture recognition<sup>33</sup> and 3D object detection<sup>34</sup>. It is important to note that PDMS, as a polymer material, may undergo aging when exposed to ultraviolet (UV) radiation. Therefore, in practical applications, appropriate encapsulation measures should be implemented, and strong UV exposure should be minimized<sup>35</sup>.  
Due to fabrication dimensional errors, particularly the lateral size deviation of PMUT generated during the back

cavity etching process and the deviation in the silicon device layer thickness, the resonant frequency of the fabricated device significantly deviates from the simulation results. In the future, process optimization will be investigated to enhance the consistency of device performance; moreover, actual process parameters can be incorporated into the simulation model to further improve its accuracy.

**Acknowledgements**  
This work is supported by the National Natural Science Foundation of China (NSFC) (12174137) and Innovation Project of Optics Valley Laboratory (Grant No. OVL2023ZD003).

**Author details**  
<sup>1</sup>School of Optical and Electronic Information, Huazhong University of Science and Technology, Wuhan 430074, China. <sup>2</sup>Optics Valley Laboratory, Hubei 430074, China. <sup>3</sup>Wuhan National Laboratory for Optoelectronics, Huazhong University of Science and Technology, Wuhan 430074, China

**Author contributions**  
Y. W. contributed to the theoretical design and acoustic performance testing of the PMUT device, as well as experimental data analysis and drafting of the manuscript. P. C. was involved in the fabrication of the PMUT device and conducted investigations related to the experimental setup. J. Z. performed the device sealing and packaging. Z. L. performed the model simulation and data curation. H. Y. proposed the original idea, supervised the study, polished the manuscript and was responsible for the funding acquisition. All the authors contributed to the article and approved the submitted version.

**Conflict of interest**  
The authors declare no competing interests.

**Supplementary information** The online version contains supplementary material available at <https://doi.org/10.1038/s41378-025-00939-x>.

Received: 21 January 2025 Revised: 3 March 2025 Accepted: 24 March 2025  
Published online: 19 May 2025

**References**  
1. Pan, J., Bai, C., Zheng, Q. & Xie, H. Review of piezoelectric micromachined ultrasonic transducers for rangefinders. *Micromachines* **14**, 374 (2023).  
2. Przybyla, R. J. et al. In-air rangefinding with an AlN piezoelectric micro-machined ultrasound transducer. *IEEE Sens. J.* **11**, 2690–2697 (2011).  
3. Luo, G. et al. Small blind-area, high-accuracy ultrasonic rangefinder using broadband multi-frequency piezoelectric micromachined ultrasonic

- transducers array. *Meas. Sci. Technol.* **34**, 125140, <https://doi.org/10.1088/1361-6501/acf682> (2023).
4. Jin, Y., Li, S., Li, J., Sun, H. & Wu, Y. Design of an intelligent active obstacle avoidance car based on rotating ultrasonic sensors. in *2018 IEEE 8th Annual International Conference on CYBER Technology in Automation, Control, and Intelligent Systems (CYBER)* 753–757 (IEEE, Tianjin, China, 2018). <https://doi.org/10.1109/CYBER2018.8688326>.
5. Tong, Z. et al. An ultrasonic proximity sensing skin for robot safety control by using piezoelectric micromachined ultrasonic transducers (PMUTs). *IEEE Sens. J.* **22**, 17351–17361 (2022).
6. Caicedo, D. & Pandharipande, A. Ultrasonic arrays for localized presence sensing. *IEEE Sens. J.* **12**, 849–858, <https://doi.org/10.1109/JSEN.2011.2161667> (2012).
7. Liu, H. et al. Drone-mounted low-frequency pMUTs for >6-meter rangefinder in air. in *2023 IEEE 36th International Conference on Micro Electro Mechanical Systems (MEMS)* 957–960 <https://doi.org/10.1109/MEMS49605.2023.10052443> (2023).
8. Przybyla, R. et al. A micromechanical ultrasonic distance sensor with >1 meter range. in *2011 16th International Solid-State Sensors, Actuators and Microsystems Conference* 2070–2073 (IEEE, Beijing, China, 2011). <https://doi.org/10.1109/TRANSDUCERS.2011.5969226>.
9. Liu, X. et al. A high-performance square pMUT for range-finder. in *2018 IEEE 13th Annual International Conference on Nano/Micro Engineered and Molecular Systems (NEMS)* 106–109 (IEEE, Singapore, 2018). <https://doi.org/10.1109/NEMS.2018.8556913>.
10. Suresh, A., Mak, K. L., Benserhir, J., Lee, J. E.-Y. & Rufer, L. Air-coupled ultrasonic rangefinder with meter-long detection range based on a dual-electrode PMUT fabricated using a multi-user MEMS process. in *2019 IEEE SENSORS* 1–4 (IEEE, Montreal, QC, Canada, 2019). <https://doi.org/10.1109/SENSORS43011.2019.8956530>.
11. Yang, H. et al. AlScN film based piezoelectric micromechanical ultrasonic transducer for an extended long-range detection. *Micromachines* **13**, 1942, <https://doi.org/10.3390/mi13111942> (2022).
12. Luo, G.-L., Kusano, Y. & Horsley, D. A. Airborne piezoelectric micromachined ultrasonic transducers for long-range detection. *J. Microelectromech. Syst.* **30**, 81–89, <https://doi.org/10.1109/JMEMS.2020.3037298> (2021).
13. Chen, X. et al. Transmitting sensitivity enhancement of piezoelectric micromachined ultrasonic transducers via residual stress localization by stiffness modification. *IEEE Electron Device Lett.* **40**, 796–799, <https://doi.org/10.1109/LED.2019.2904293> (2019).
14. Ledesma, E., Zamora, I., Uranga, A. & Barniol, N. Tent-plate AlN PMUT with a piston-like shape under liquid operation. *IEEE Sens. J.* **20**, 11128–11137, <https://doi.org/10.1109/JSEN.2020.2995643> (2020).
15. Qu, M., Chen, X., Zhu, K., Guo, X. & Xie, J. Beam-membrane coupled piezoelectric micromachined ultrasonic transducers with enhanced transmitting sensitivity. *Micromachines* **13**, 423, <https://doi.org/10.3390/mi13030423> (2022).
16. Wang, Y., Chen, P., Zhang, J. & Yu, H. Quasi-closed diaphragm based piezoelectric micromachined ultrasonic transducer with reduced Q and stress sensitivity for in-air rangefinding. *Sens. Actuator A* **379**, 115938, <https://doi.org/10.1016/j.sna.2024.115938> (2024).
17. Gong, Y. et al. Piezoelectric micromachined ultrasonic transducers with superior frequency control. *J. Microelectromech. Syst.* **32**, 6, <https://doi.org/10.1109/JMEMS.2023.3305461> (2023).
18. Gong, Y. et al. Ultrahigh-sensitivity coupled cantilever and dual-cavity piezoelectric micromachined ultrasonic transducers. *IEEE Electron Device Lett.* **45**, 5, <https://doi.org/10.1109/LED.2024.3375956> (2024).
19. Trivedi, S. et al. Curved cantilever actuated ScAlN PMUT for Enhanced Linearity and Transmit Sensitivity. in *2024 IEEE Ultrasonics, Ferroelectrics, and Frequency Control Joint Symposium (UFFC-JS)* 1–4 (IEEE, Taipei, Taiwan, 2024). <https://doi.org/10.1109/UFFC-JS60046.2024.10794053>.
20. Guedes, A. et al. Aluminum nitride pMUT based on a flexurally-suspended membrane. in *2011 16th International Solid-State Sensors, Actuators and Microsystems Conference* 2062–2065 (IEEE, Beijing, China, 2011). <https://doi.org/10.1109/TRANSDUCERS.2011.5969223>.
21. Wang, Y., Lv, T., Zhang, J. & Yu, H. Capillary effect-based selective sealing strategy for increasing piezoelectric MEMS speaker performance. *Microsyst. Nanoeng.* **10**, 108, <https://doi.org/10.1038/s41378-024-00753-x> (2024).
22. Berthier, J. et al. The dynamics of spontaneous capillary flow in confined and open microchannels. *Sens. Transducers* **183**, 123 (2014).
23. Timoshenko S. P., Young D. H. & Weaver W. *Vibration Problems in Engineering*, 4th edn. Ch. 1 (John Wiley & Sons, 1974).
24. Hosseini, R. & Hamed, M. Study of the resonant frequency of unimorph triangular V-shaped piezoelectric cantilever energy harvester. *Int. J. Adv. Manuf. Technol.* **8**, 75–82 (2015).
25. Liu, C. et al. Ultrahigh-sensitivity piezoelectric AlN MEMS speakers enabled by analytical expressions. *J. Microelectromech. Syst.* **31**, 664–672 (2022).
26. Du, G., Zhu, Z. & Gong, X. *Fundamentals of Acoustics*, 3rd edn. Ch. 6 (Nanjing University Press, 2012).
27. Berthier, J. et al. Suspended microflows between vertical parallel walls. *Microfluid. Nanofluid.* **18**, 919–929 (2015).
28. Bass, H. E., Sutherland, L. C., Zuckerwar, A. J., Blackstock, D. T. & Hester, D. M. Atmospheric absorption of sound: Further developments. *J. Acoustical Soc. Am.* **97**, 680–683, <https://doi.org/10.1121/1.412989> (1995).
29. Velasco, S. et al. A computer-assisted experiment for the measurement of the temperature dependence of the speed of sound in air. *Am. J. Phys.* **72**, 276–278 (2004).
30. Przybyla, R., Izyumin, I., Kline, M., Boser, B. & Shelton, S. An ultrasonic rangefinder based on an AlN piezoelectric micromachined ultrasound transducer. in *2010 IEEE Sensors* 2417–2421 (IEEE, Kona, HI, 2010). <https://doi.org/10.1109/ICSENS.2010.5690777>.
31. Alasatri, S., Rufer, L. & Lee, J. E.-Y. AlN-on-Si square diaphragm piezoelectric micromachined ultrasonic transducer with extended range of detection. in *EURO-SENSORS 2018* 913 (MDPI, 2018). <https://doi.org/10.3390/proceedings2130913>.
32. Pala, S., Shao, Z., Peng, Y. & Lin, L. Improved ring-down time and axial resolution of pMUTs via a phase-shift excitation scheme. in *2021 IEEE 34th International Conference on Micro Electro Mechanical Systems (MEMS)* 390–393 (IEEE, Gainesville, FL, USA, 2021). <https://doi.org/10.1109/MEMS1782.2021.9375227>.
33. Przybyla, R. J., Tang, H. Y., Shelton, S. E., Horsley, D. A. & Boser, B. E. 3D ultrasonic gesture recognition. in *IEEE International Solid-State Circuits Conference Digest of Technical Papers (ISSCC)* 210–211 (IEEE, 2014).
34. Shao, Z., Peng, Y., Pala, S., Liang, Y. & Lin, L. 3D ultrasonic object detections with >1 meter range. in *2021 IEEE 34th International Conference on Micro Electro Mechanical Systems (MEMS)* 386–389 (IEEE, Gainesville, FL, USA, 2021). <https://doi.org/10.1109/MEMS1782.2021.9375173>.
35. Charitidis, C. A. et al. Influence of accelerated aging on nanomechanical properties, creep behaviour and adhesive forces of PDMS. *Plast. Rubber Compos.* **41**, 94–99 (2012).